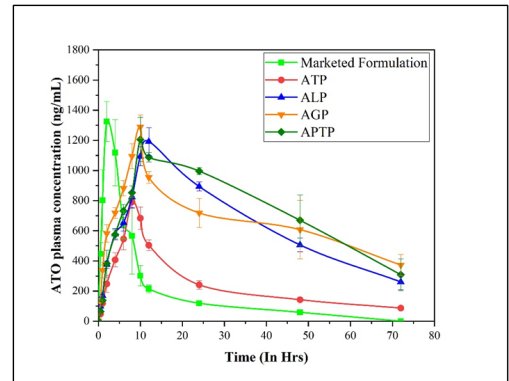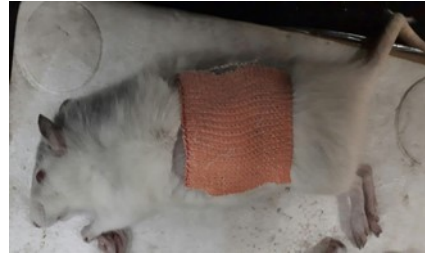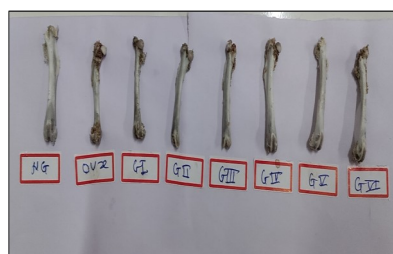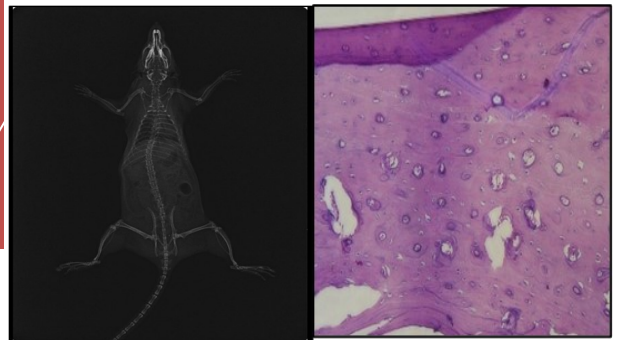Pharmacokinetic study

Chapter-10

In vivo studies

Pharmacodynamic study

10.1. Introduction:

The most popular alternative to the oral route, i.e., the transdermal route, has been investigated in order to solve gastrointestinal issues with the currently marketed formulations of both ATO and RSNa. As mentioned in the previous chapter, transdermal patches with integrated nanocarriers were successfully developed, tested for in vitro as well as ex vivo characteristics, and found to be most suitable for transdermal distribution. This chapter describes the pharmacokinetic (PK) and pharmacodynamic (PD) effects of the developed formulations of ATO and RSNa.

10.2. Materials and methods:

10.2.1. Materials:

Marketed formulations of ATO and RSNa, Xylazine, ketamine, tramadol, Neosporin powder and other surgical related products were purchased from local medical stores. Serum calcium detection kit was purchased from Span Diagnostic Ltd., Surat, India. Serum inorganic phosphorous detection kit was purchased from Beacon diagnostic Pvt. Ltd., Navsari, India.

10.2.2. Animal study protocol approval:

The Committee for Purpose of Control and Supervision of Experiments on Animals (CPCSEA), Ministry of Social Justice and Empowerment, Government of India, guidelines were used for performing the in vivo studies. Approval was taken from the Institutional Animal Ethics Committee (IAEC) of the Faculty of Pharmacy, Maharaja Sayajirao University of Baroda, Vadodara, India, for the protocols of both pharmacokinetic and pharmacodynamic studies with protocol no. MSU/IAEC/2021-22/2110.

10.2.3. Animal Procurement:

Female adult Sprague Dawley (SD) rats weighing between 150 - 250 g were obtained from Zydus Research Centre, Ahmedabad. The rats were housed in suitable cages at the G. H. Patel Pharmacy Building, The Maharaja Sayajirao University of Baroda, Vadodara (registration number: 404/PO/Re/S/01/CPCSEA; dated October 28, 2015), and remained under quarantine for 15 days and fed commercial pelleted rat food (VRK nutritional solution, Keval Sales Corporation,

Vadodara) and RO water. With a 12-hour light-dark cycle and housing three animals per cage at a temperature of 20–24°C, the animals had free access to food and water.

10.3. In vivo pharmacokinetic studies:

For the pharmacokinetic investigation, rats were divided into 10 groups of 6 animals per group at random, as shown in the table-10.1.

Table-10.1. Study design for pharmacokinetic study

Groups	Sample	Route of administration	Dose
Group-I	ATO Marketed formulation (AMF)	Oral	20 mg/kg
Group-II	ATO loaded transdermal patches (ATP)	Transdermal	20 mg/kg
Group-III	ATO loaded liposomal transdermal patches (ALP)	Transdermal	20 mg/kg
Group-IV	ATO loaded glycerosomal transdermal patches (AGP)	Transdermal	20 mg/kg
Group-V	ATO-PECN loaded transdermal patches (APTP)	Transdermal	20 mg/kg
Group-VI	RSNa Marketed formulation (RMF)	Oral	1.5 mg/kg
Group-VII	RSNa loaded transdermal patches (RTP)	Transdermal	1.5 mg/kg
Group-VIII	RSNa loaded liposomal transdermal patches (RLP)	Transdermal	1.5 mg/kg
Group-IX	RSNa loaded glycerosomal transdermal patches (RGP)	Transdermal	1.5 mg/kg
Group-X	RSNa-PECN loaded transdermal patches (RPTP)	Transdermal	1.5 mg/kg

10.3.1. Sample administered:

The oral administration was carried out using an oral feeding needle (16 gauge), and the transdermal patch was applied using Medigrip elastic adhesive bandage B.P. (Medigrip, Precision Coating Ltd., India).

10.3.2. Blood sample collection:

Following dosing, blood was collected from the retro-orbital plexus (not more than 0.5 mL) from the animals in Eppendorf's tubes containing 50 µL of disodium EDTA solution at predetermined intervals (0.5, 1, 2, 4, 6, 8, 10, 12, 24, 48, and 72 hrs). The plasma was separated at 10°C for 15 minutes at 10000 rpm and stored at -20°C until further analysis [1, 2].

10.3.3. Preparation of sample for analysis:

a. Extraction of ATO from plasma:

Aliquots of 200 µL of plasma were taken in eppendorf, and the volume was made up to 1 mL with acetonitrile for each sample to precipitate plasma proteins. The mixture was centrifuged at 5000 rpm for 10 minutes. The obtained supernatant was separated, filtered through 0.22 µm syringe filters, and collected in another Eppendorf tube. After that, the samples were injected into HPLC for analysis as described in chapter-3 [1-4].

b. Extraction of RSNa from plasma:

200 µL aliquots of plasma were collected and diluted with 1.4 mL of double-distilled water in Eppendorf tubes. The sample was deproteinized by adding 450 µL of 10% (w/v) trichloroacetic acid (TCA) slowly while vortexing, followed by a 15-minute centrifugation at 1500 rpm at 25°C. The supernatant was collected in another eppendorf, and a freshly prepared 50 µL aliquot of 1.25 M $CaCl_2$ and 57 µL of 30% (w/v) NaOH were added, which formed a visible white precipitate. The sample was thoroughly mixed using a vortex mixer before being centrifuged at 5000 RPM for 10 minutes. The supernatant was removed and the pellet was dissolved in 400 µL of 1M HCl and heated on a water bath for 30 minutes at 90±5°C to hydrolyze any pyrophosphate in the plasma. Additional 25 µL of 1.25M

CaCl$_2$ was added, followed by 90 µL of 30% NaOH, and centrifuged at 5000 RPM for 10 minutes. The pellet was dissolved in 50 µL of 1M HCl before being diluted in 2 mL of deionized water. With the addition of 45 µL of 30% NaOH, a little white precipitate formed, and the sample was centrifuged at 5000 RPM for 10 minutes. The precipitate was dissolved in 80 µL of 0.025M disodium EDTA and volume make up with mobile phase to 1 mL, vortexed for 1-2 minutes, filtered through a 0.45 µm syringe filter, and HPLC analysis was performed as described in chapter-3 [5-8].

10.3.4. Analysis of pharmacokinetic parameters:

The different pharmacokinetic parameters, viz., C$_{max}$ (maximum concentration in plasma), T$_{max}$ (time required to reach maximum concentration in plasma), area under the curve (AUC), half-life (t$_{1/2}$), mean residential time (MRT), etc., were analyzed by non-compartmental analysis using Kinetica version 5.0.11 pharmacokinetic software (PK-PD analysis, Thermofischer Scientific). The graph of plasma drug concentration versus time was plotted for all groups. The relative bioavailability of developed formulations was compared with that of marketed formulation [1, 9-12].

10.4. In vivo pharmacodynamic studies:

Animal osteoporosis models can be used to confirm in vivo treatment efficacy. Ovariectomy-induced osteoporosis, glucocorticoid-induced osteoporosis, alcohol-abuse osteoporosis, fracture repair models, genetic models, orthotopic formation of bones models, immobilisation models, and so on are a few examples [13, 14]. Several aspects influence model selection and animal species selection, including illness condition simulation, variations in animal and human physiology, animal size, gender, and age, ease and time for osteoporosis induction, and so on. Among these models, ovariectomy-induced osteoporosis has been widely recognised as a good model for improving osteoporosis induction and evaluating the antiosteoporotic efficacy of drug-loaded formulations [15, 16]. Specifically, ovariectomized rats have severe cancellous (spongy) and cortical bone loss [13]. Cancellous bone loss after ovariectomy in rapidly growing rats is caused mostly by altered growth of bones [13, 17-19]. On the other hand, ovariectomy causes cancellous and cortical bone loss in mature rats (rats with

mature skeletal development) via a different mechanism, namely abnormal bone remodelling [13, 19, 20].

An ovariectomized female Sprague Dawley rat model was used in this study for evaluating the therapeutic potential of ATO and RSNa loaded nanocarriers' anti-osteoporotic activity. Different treatments were administered to osteoporosis-induced rats, and various evaluation parameters were used to monitor cancellous and cortical bone changes.

10.4.1. Induction of osteoporosis:

Ovariectomy surgery:

The surgery was performed under aseptic conditions under anaesthesia. Bilateral ovariectomy was performed in rats following the method of Abiramasundari *et al*. 2017 [15, 21-25]. After intraperitoneal injections of xylazine (80 mg/kg body weight) and ketamine hydrochloride (20 mg/kg body weight) anaesthesia, the surgery was done through two separate flank incisions. For the flank incisions, the animal was placed on her side. A 1.5-2 cm incision was cut in the skin, and the periovarian fatty tissue was retrieved and identified. With blunt forceps, the ovary was gently dragged out via the incision by grabbing the fat pad around it. A haemostat was put at the oviduct-uterus junction, a ligature was placed just below the haemostat (close to the uterus), and an incision was made immediately above the haemostat. After removing the ovary and oviduct, the haemostat was released and haemostasis checked before releasing the uterus and allowing it to return to the abdomen. The oviduct and skin were ligated using sterile surgical braided silk suture 4/0 (NW-5050, Mersilk, Ethicon manufacturing Pvt. Ltd, Johnson and Johnson Pvt. Ltd. India). The animal was kept under observation for the next 24 hours after surgery. Tramadol was administered intraperitoneally after surgery to relieve pain. The animals tolerated the surgery well, and the post-operative recovery was uncomplicated. Post-operative treatment included prevention to avoid infection and the application of antibiotic powder (Neosporin) to the surgical site as necessary until they recovered.
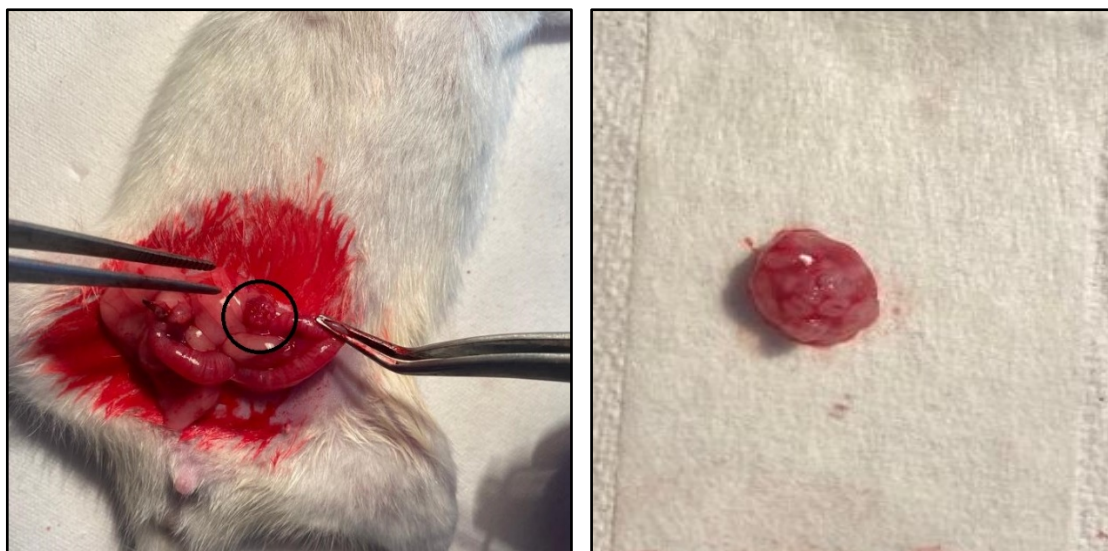
a. Site of ovary in rat   b. Isolated ovary

Figure- 10.1. Bilateral ovariectomy surgery.

10.5. Antiosteoporotic treatment:

In the pharmacodynamic study, female Sprague Dawley (SD) rats weighing 230-280 g were used. Rats were randomly separated into 8 groups (each group including 6 animals) for the pharmacodynamic study, as shown in the table- 10.2.

Table-10.2. Study design for pharmacodynamic study

Groups	Sample	Route of administration	Dose
Group-I (NG)	Normal Group	-	-
Group-II (OG)	Ovariectomized (disease) Model	-	-
Group-III (G-I)	Ovariectomy + ATO Marketed formulation	Oral	20 mg/kg
Group-IV (G-II)	Ovariectomy + ATO loaded glycerosomal transdermal patches (AGP)	Transdermal	20 mg/kg
Group-V (G-III)	Ovariectomy + ATO-PECN loaded transdermal patches (APTP)	Transdermal	20 mg/kg
Group-VI (G-IV)	Ovariectomy + RSNa Marketed formulation	Oral	1.5 mg/kg
Group-VII (G-V)	Ovariectomy + RSNa loaded glycerosomal transdermal patches (RGP)	Transdermal	1.5 mg/kg
Group-VIII (G-VI)	Ovariectomy + RSNa-PECN loaded transdermal patches (RPTP)	Transdermal	1.5 mg/kg

10.6. Evaluation of Antiosteoporotic activity:

1. Radiological analysis:

After 30 days of treatment, the rats were anaesthetized with ether in a closed chamber. Following the anaesthetic procedure, the animal was subjected to whole-body radiographs using an X-ray scanner (foX-Rayzor) [X-rays were taken at Angela Lobo Clinic, Vadodara]. X-rays were used to expose samples for 10 milliseconds at a working distance of 35 inches from the X-ray emitters. The untreated control animals'

Faculty of Pharmacy, The MS University of Baroda.
Pravin Yadav Patil / 2023.

391

bone macroarchitecture was compared to the ovariectomized and treated groups [24, 26-28].

2. Bone weight, bone volume and bone density:

After treatment, all rats were sacrificed by euthanizing them humanely by overdosing diethyl ether inhalation, and the femur bone of every rat was removed for further analysis.

The femur of all rats was subjected to weight, which was measured by a digital weighing balance, and the length of the bone was measured by a calibrated measuring scale. Bone weight/mm was calculated and compared with the bone weight of the normal and OVX group. The volume of bone samples was recorded by plethysmometer in 0.45 % saline solution. Bone density of bone samples were recorded by Archimedes principle where bone weight was divided from bone volume to calculate bone density [29-31].

3. Biochemical assay:

A. Blood sample collection and serum separation:

After treatment, blood was collected from the retro orbital plexus of each group of rats. Serum was collected from these blood samples by centrifugation at 5000 rpm for 15 minutes. The serum was separated carefully and kept at -20 °C until further study. The serum samples were then used for biochemical analysis.

B. Estimation of serum calcium:

The estimation of serum calcium was carried out by modified O-cresolphthalein complexone method [32-36]. In a nutshell, 20 µL of test samples were mixed to 1 mL of calcium reagent containing O-cresolphthalein complexone. Calcium forms a bluish-purple complex with O-cresolphthalein complexone in alkaline solution; this complex is detectable using a semi-automatic analyzer at 578 nm. The standard was prepared in the same manner as the test samples in a separate tube. The amount of colour produced is directly related to the sample's calcium content, which is measured in mg/dL. Using a standard biochemical kit obtained from

Span Diagnostic Ltd. (Surat, India), the serum samples' calcium concentrations were determined using the formula:

$$\text{Serum Calcium (mg/dL)} = \frac{\text{Absorbance of Test}}{\text{Absorbance of Standard}} \times 10$$

……………………………….. equation-10.1

C. Serum inorganic phosphorous:

The estimation of serum phosphorus was carried out by the phosphomolybdate complex method [36-40]. In a nutshell, 10 µL of test samples were mixed with 1 mL of molybdate reagent. Ammonium molybdate and inorganic phosphorus combine to form phosphomolybdate complex. Using a semi-automatic analyzer, this phosphomolybdate complex is measured at 340 nm and is directly proportional to the sample's inorganic phosphate concentration, which is given in mg/dL. Using a standard biochemical kit obtained from Beacon Diagnostic Ltd. (Navsari, India), the quantity of inorganic phosphate found in the serum samples was determined using the following formula:

$$\text{Serum inorganic phosphorous (mg/dL)} = \frac{\text{Absorbance of Test}}{\text{Absorbance of Standard}} \times 5$$

……………………………….. equation-10.2

4. Histopathology of bone sample:

After treatment, rats were sacrificed by overdose inhalation of diethyl ether, and femur bones were removed. The collected bone samples of normal group, OVX group and treated group were subjected for histopathological study. For histological evaluation, the bone samples were fixed in 10% paraformaldehyde in phosphate buffered saline (PBS) for 16 hours at 4°C. Femur samples were decalcified in 10% EDTA, dehydrated, and embedded in paraffin after fixing. An inverted microscopy (Nikon Ti2E, USA) was used for examining paraffin embedded horizontal bone slices of 5 µm thickness taken from the femur head (the bone component towards the hip joint) [16, 36, 41-45].

10.7. Results and discussion:

10.7.1. In vivo pharmacokinetic study:

a. ATO loaded formulations:

The concentration of ATO in blood plasma of rats was determined and data are represented in table- 10.3. The plot of ATO plasma concentration with function of time is represented in figure-10.2. The thermo scientific^{TM} Kinetica software was utilized for the calculation of various pharmacokinetic parameters as represented in table- 10.4.

Table- 10.3. Plasma concentration of ATO vs time profile.

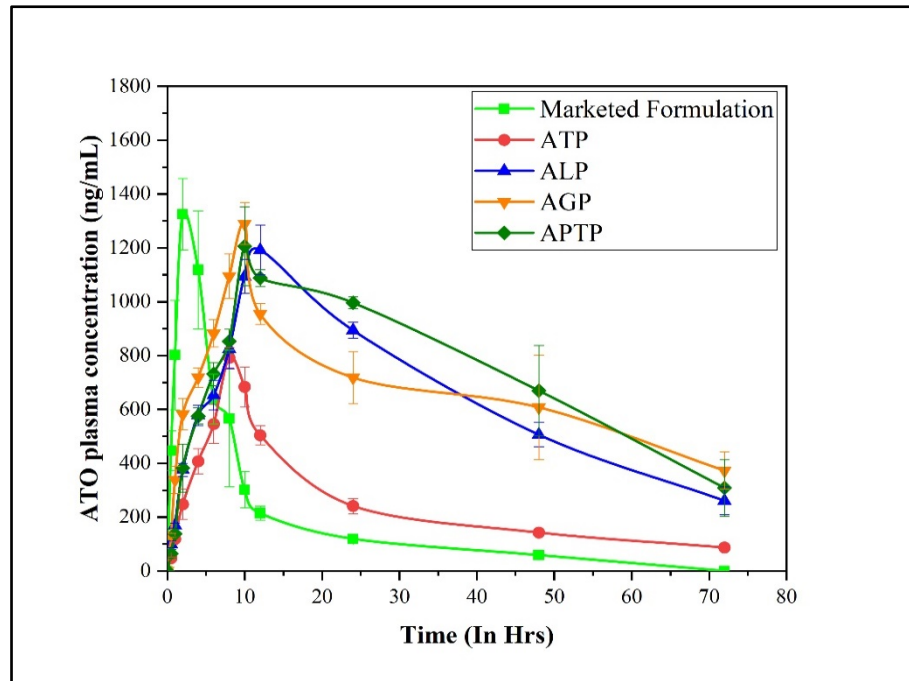| Time (In hrs)	Plasma concentration (ng/mL)				
	Marketed formulation (Oral)	ATP	ALP	AGP	APTP
		Transdermal			
0	0.00 ± 0.00	0.00 ± 0.00	0.00 ± 0.00	0.00 ± 0.00	0.00 ± 0.00
0.5	446.82 ± 34.26	47.30 ± 4.12	98.59 ± 9.48	132.08 ± 11.56	64.74 ± 15.68
1	801.37 ± 82.31	118.46 ± 8.93	169.51 ± 12.26	338.51 ± 75.09	137.81 ± 9.26
2	1325.11 ± 72.62	247.48 ± 55.74	375.75 ± 24.04	582.25 ± 86.01	382.29 ± 89.93
4	1117.77 ± 118.57	407.29 ± 46.37	578.64 ± 37.17	719.18 ± 53.90	575.18 ± 30.31
6	638.24 ± 92.36	545.91 ± 71.84	652.79 ± 54.96	882.25 ± 76.38	731.76 ± 42.41
8	565.74 ± 53.10	792.13 ± 37.32	824.80 ± 73.32	1095.19 ± 24.25	853.10 ± 44.36
10	301.10 ± 67.57	683.90 ± 73.74	1093.76 ± 62.81	1289.84 ± 46.16	1205.95 ± 45.75
12	214.44 ± 26.18	504.28 ± 35.19	1192.08 ± 92.65	954.68 ± 57.96	1088.60 ± 31.29
24	119.29 ± 3.72	241.18 ± 27.84	893.98 ± 30.07	718.27 ± 46.10	996.24 ± 21.93
48	59.10 ± 7.87	142.69 ± 7.46	506.17 ± 44.89	607.47 ± 29.37	669.74 ± 68.00
72	ND	87.09 ± 8.99	260.87 ± 51.24	373.06 ± 54.01	308.43 ± 53.40

Figure- 10.2. ATO plasma concentration vs time profile

Table- 10.4. Pharmacokinetic parameters of ATO loaded formulations

Parameters	Marketed formulation (oral)	ATP	ALP	AGP	APTP
		Transdermal			
C_{max} (ng/mL)	1385.65 ± 72.62	792.12 ± 37.32	1192.07 ± 62.65	1289.83 ± 46.16	1205.37 ± 45.75
T_{max} (Hr)	2.66 ± 1.55	8.00 ± 0.00	12.00 ± 0.00	10.00 ± 0.00	11.33 ± 1.15
AUC_{0-72} (ng*hr/mL)	14548.91 ± 176.61	21498.61 ± 567.19[*]	56257.60 ± 2646.87[*,#]	73204.60 ± 2990.43[*,#]	69378.82 ± 1600.69[*,#]
$t_{1/2}$ (Hr)	20.12 ± 2.23	33.16 ± 4.63	27.50 ± 4.93	47.78 ± 11.44	33.95 ± 4.94
MRT (Hr)	19.69 ± 2.38	43.63 ± 4.72	44.99 ± 7.24	69.96 ± 14.70	55.40 ± 10.21
Relative bioavailability (Folds)	1	1.47	3.87	5.03	4.76

* $p < 0.05$ as compared to marketed formulation,

# $p < 0.05$ as compared to ATP.

When the marketed formulation of ATO i.e., suspension of tablet in distilled water was administered orally to rats through oral route, maximum concentration (C_{max}) was found to be 1385.65 ± 72.62 ng/mL, with T_{max} of 2.66 ± 1.55 hr and half-life was found to be 20.12 ± 2.23 hr with 19.69 ± 2.38 hr of MRT. The poor AUC in oral marketed formulation is due to first pass metabolism and poor absorption of drug through GIT. The pharmacokinetic parameters in transdermal formulations such ATP, ALP, AGP, and APTP showed a significant difference ($p < 0.05$). ATP showed lower C_{max} and AUC indicating poor permeability of ATO through skin. The permeation of drug through skin was improved by incorporation of drug into nanocarriers. The nanocarriers incorporated transdermal patch showed significant ($p < 0.05$) improvement in C_{max} and AUC than marketed oral formulation and ATP.

ALP showed C_{max} of 1192.07 ± 92.65 ng/mL with 56257.60 ± 2646.87 ng*hr/mL of AUC, while, the AGP showed 1289.83 ± 46.16 ng/mL of C_{max} and 73204.60 ± 2990.43 ng*hr/mL of AUC. Based on PK parameters, it was observed that AGP improved bioavailability as compared to oral marketed formulation, ATP, and ALP due to the presence of permeation-enhancer vesicle (glycerosomes) and its elastic properties enhanced the permeation of drug through skin and reached to systemic circulation. There was a significantly ($p<0.05$) increased AUC of AGP, which revealed the enhancement of the bioavailability of the drug as compared to the marketed formulation, ATP, and ALP. The bioavailability of ATO from AGP was enhanced 5.03-, 3.40-, and 1.30- folds as compared to oral marketed formulation, ATP, and ALP respectively. Due to enhancement in relative bioavailability of developed formulation, there is chance of dose reduction upto > 3-5- folds. This indicates the possibility of reduction in dose and consequently the side effects of ATO.

In case of ATO-PECN incorporated transdermal patch, the C_{max} was found to be 1205.37 ± 45.75 ng/mL with AUC of 69378.82 ± 1600.69 ng*hr/mL. The APTP showed significant ($p<0.05$) increase in AUC as compared to ATP and marketed oral formulation. The bioavailability of APTP was enhanced 4.76- and 3.22- folds as compared to marketed formulation and ATP respectively. The increase in the AUC suggested the enhancement of permeation of drug through skin from APTP due to the nanosize of formulation and hydrating nature of chitosan. The high positive surface

charge on particles and presence of permeation enhancer (glycerol) in transdermal patch significantly enhanced the permeation of drug through skin and enabled it to reach systemic circulation.

b. RSNa loaded formulation:

The concentration of ATO in blood plasma of rats was determined and data are represented in table- 10.5. The plots of RSNa plasma concentration vs time are represented in figure- 10.3. The various pharmacokinetic parameters are represented in table- 10.6.

After oral administration of RSNa tablet, the C_{max} was found to be 442.53 ± 54.19 ng/mL with 2403.61 ± 60.36 ng*hr/mL of AUC. According to the results, the C_{max} from RSNa tablet was low due to poor absorption from GIT attributed to RSNa forming a complex with divalent cations such as calcium, magnesium, and others resulting in poor bioavailability [12, 46].

The transdermal formulation showed significantly ($p<0.05$) better controlled plasma levels with sustained release having half-life ranging from 18-47 hr with 24-73 hr of MRT. RTP exhibited lowest C_{max} and AUC due to poor permeability of drug through skin. RLP showed 572.67 ± 40.90 ng/mL of C_{max} and 28217.87 ± 904.97 ng*hr/mL of AUC, while RGP showed 645.46 ± 32.16 ng/mL of C_{max} and 44395.51 ± 2568.00 ng*hr/mL of AUC. From the results, it showed that an increase in the AUC of RGP as compared to RLP and RTP due to an increase in the permeation of the drug through the skin and the maximum amount of drug reaching systemic circulation. The increase in permeation of drug through skin is due to nanosize and deformable nature of glycerosomes which easily pass through skin and reaches to systemic circulation as compared to RTP and RLP. The increased water content in the dense connective dermal layer promotes hydration and relaxation due to the presence of glycerol, which therefore makes it easier for glycerosomal formulation to diffuse through the skin layer [47-50]. The bioavailability of RGP was increased 18.47-, 7.42- and 1.57- folds as compared to marketed formulation, RTP and RLP respectively. This increase in bioavailability of developed formulation indicated the possibility of dose reduction and consequently the side effects.

Table- 10.5. Plasma concentration of RSNa vs time profile.

| Time (In hrs)	Plasma concentration (ng/mL)				
	Marketed formulation (Oral)	RTP	RLP	RGP	RPTP
		Transdermal			
0	0.00 ± 0.00	0.00 ± 0.00	0.00 ± 0.00	0.00 ± 0.00	0.00 ± 0.00
0.5	188.52 ± 15.71	ND	0.00 ± 0.00	71.54 ± 9.42	0.00 ± 0.00
1	309.33 ± 27.74	ND	95.90 ± 13.15	98.04 ± 8.70	84.75 ± 8.19
2	442.53 ± 54.19	ND	206.96 ± 47.10	164.51 ± 30.18	148.60 ± 7.76
4	267.73 ± 39.90	106.95 ± 7.98	277.13 ± 46.38	247.80 ± 31.54	225.76 ± 24.51
6	166.34 ± 5.96	143.84 ± 4.56	334.54 ± 34.79	322.37 ± 31.32	296.62 ± 32.13
8	94.13 ± 3.83	280.56 ± 28.55	408.00 ± 28.02	408.00 ± 28.02	408.00 ± 28.02
10	31.68 ± 4.35	230.92 ± 33.00	572.67 ± 40.90	645.46 ± 32.16	543.50 ± 43.36
12	ND	147.14 ± 5.10	471.51 ± 28.93	603.66 ± 42.23	425.19 ± 43.97
24	ND	119.65 ± 25.46	380.09 ± 45.48	472.37 ± 21.31	342.32 ± 32.28
48	ND	ND	248.58 ± 48.37	374.97 ± 25.57	217.47 ± 30.10
72	ND	ND	141.36 ± 9.34	243.16 ± 44.72	167.55 ± 20.77
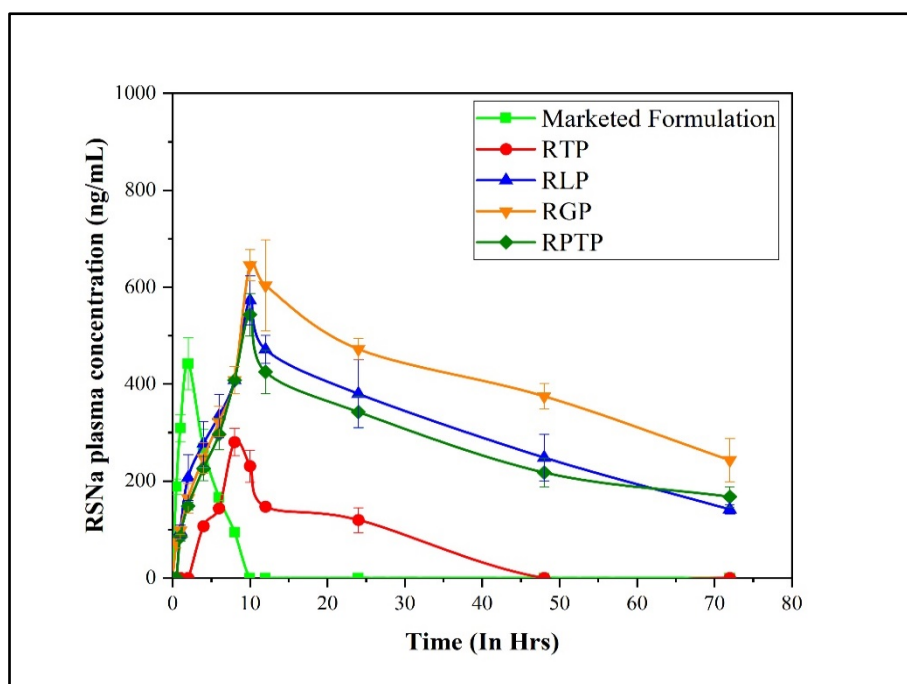
Figure- 10.3. RSNa plasma concentration vs time profile

Table- 10.6. Pharmacokinetic parameters of RSNa loaded formulations

Parameters	Marketed formulation (oral)	RTP	RLP	RGP	RPTP
			Transdermal		
C_{max} (ng/mL)	442.53 ± 54.19	280.56 ± 28.55	572.67 ± 40.90	645.46 ± 32.16	543.50 ± 43.36
T_{max} (Hr)	2.00 ± 0.00	8.00 ± 0.00	10.00 ± 0.00	10.00 ± 0.00	10.00 ± 0.00
AUC_{0-72} (ng*hr/mL)	2403.61 ± 160.36	6002.75 ± 1396.01[*]	28217.87 ± 904.97[*,#]	44395.51 ± 2568.00[*,#]	30174.33 ± 3825.76[*,#]
$t_{1/2}$ (Hr)	2.12 ± 0.23	18.78 ± 3.00	37.09 ± 10.34	46.57 ± 6.76	44.16 ± 4.72
MRT (Hr)	4.16 ± 0.07	24.56 ± 12.29	56.75 ± 12.39	72.37 ± 9.11	68.54 ± 6.05
Relative bioavailability (Folds)	1	2.50	11.73	18.47	12.55

* p < 0.05 as compared to marketed formulation

# p < 0.05 as compared to RTP.

The PK results of RPTP showed 543.50 ± 43.36 ng/mL of C_{max} with 30174.33 ± 3825.76 ng*hr/mL of AUC. The RPTP showed a 5.02- and 12.55-fold significant enhancement ($p < 0.05$) in bioavailability as compared to the RTP and marketed formulation, respectively. The enhancement in bioavailability of RPTP is due to the nanosized chitosan-based nanoparticles with permeation enhancer (glycerol) which hydrates stratum corneum and highly positively surface charge which facilitated the permeation of drug through skin layers and enabled it to reach systemic circulation. The enhancement in bioavailability indicates the possibility of reduction in dose.

10.7.2. In vivo pharmacodynamic studies:

Evaluation of Antiosteoporotic activity:

10.7.2.1. Radiological analysis:

The X-ray radiograph of the rats of different treatment groups are shown in the figure-10.4. The X-ray radiograph of the ovariectomized rats (figure- 10.4B) show significantly reduced radio-opacity as compared to normal group (figure-10.4A). When compared to the normal group, the radio-opacity of the OVX group was found to be less intense and faint. The region of femur and tibia bone joint were found to be distorted indicating and confirming the osteoporosis induction in OVX group. The ovariectomy surgery is known to accentuate the osteoclast activity and resorption of bone, thereby preventing the new bone formation, and accelerating the bone erosion [51]. This indicates the development of osteoporosis after ovariectomy. As it can be seen in the figure-10.4C-H, the treated rats showed increase in the radiopacity of bone as compared ovariectomized rat. The orally administered ATO (C) and RSNa (F) treated rats showed slight increase in the radio-opacity of bone as compared to OVX group. This happened due to the low oral bioavailability of ATO as well as RSNa, which showed less effectiveness of the drug for the treatment of osteoporosis. After treatment of nanocarriers loaded transdermal patches, the X-ray radiography of rats showed significant enhancement in the radio-opacity of bones (D, E, G and H) as compared to orally treated rats (C and F) and OVX group. This happened due to the enhancement of the bioavailability of the drug from the nanocarrier-loaded transdermal patch, which helps to increase bone formation and reduce

bone resorption, resulting in anti-osteoporotic activity. The increased radiopacity in the region of bone epiphysis, metaphysis and bone shaft region of rats was observed after the treatment with nanocarriers loaded transdermal patch. The ATO loaded nanocarriers incorporated transdermal patch treated rats also showed significant increase in the radio-opacity of bones as like RSNa loaded nanocarriers incorporated transdermal patch. Hence, on the basis of results it was observed that ATO also helps to reduce bone resorption and increase the bone formation by inducing osteoclast activity and increasing activity of osteoblast, resulting in increase in bone mass. The RSNa-loaded nanocarriers permeated a higher amount of the drug through the skin to the trabeculae of the bone, where the osteoclastic effects must have been inhibited by risedronate conjugation with the hydroxyapatite content of the bones, which in turn triggered an enhanced reformation of the bone and of the cortical line with the action of osteoblasts. In the case of nanocarrier-incorporated transdermal patches treated groups, the joint between the femur and tibia was found to be less distorted (highly radiopaque) than in the OVX group and orally administered drug treated groups.
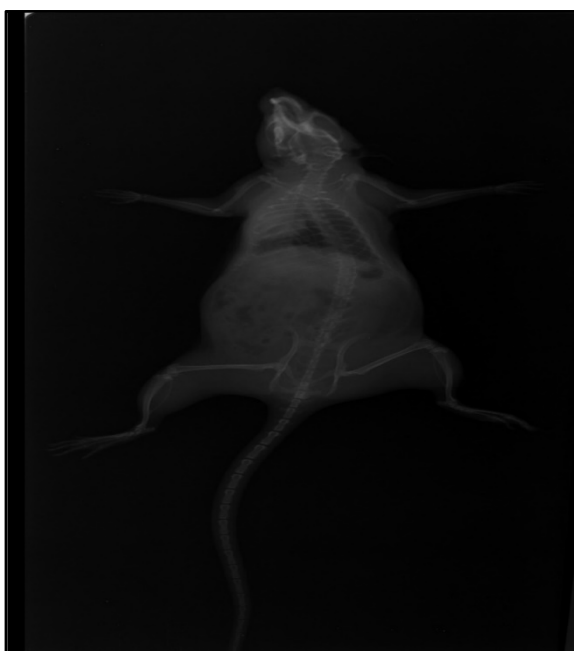
The results indicated that the prepared formulations were able to induce bone formation and reduced bone resorption in osteoporotic rats as compared to orally administered drug. The results concluded the effectiveness of the developed AGP, RGP, APTP and RPTP for treatment of osteoporosis through transdermal administration.
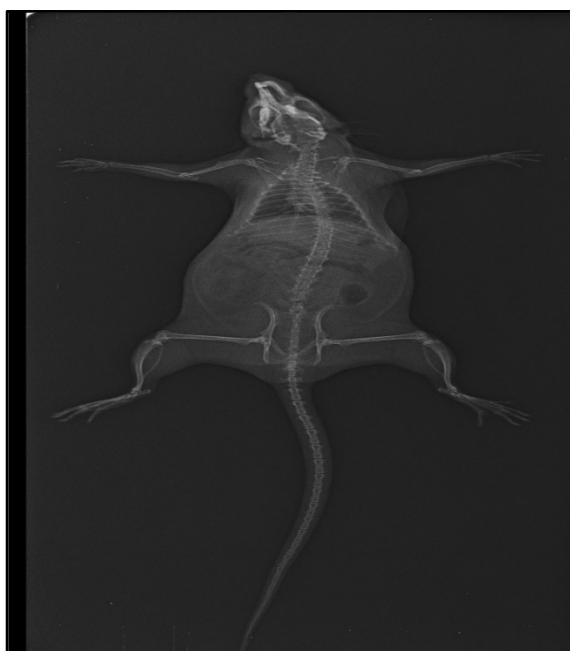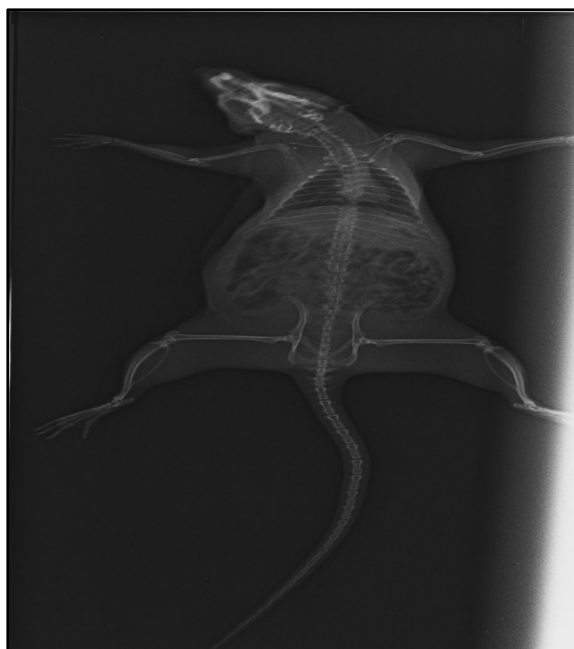
A.   Normal Group (NG)

B.   OVX group (OG)

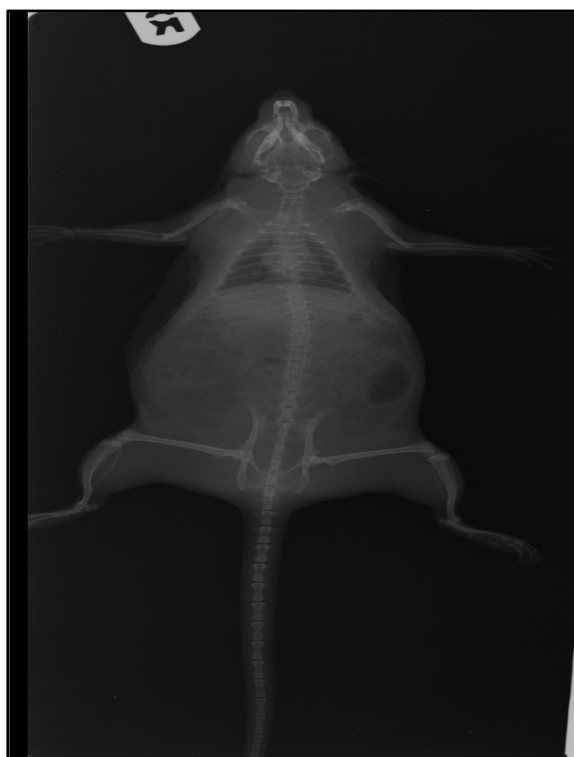
C. ATO- Marketed formulation (Group-I)
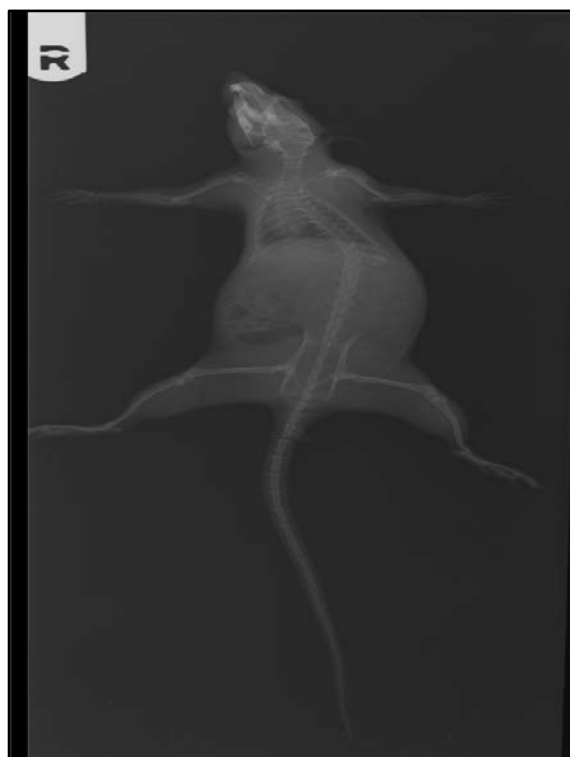

D. AGP (Group-II)

E. APTP (Group-III)

F. RSNa- Marketed formulation

(Group-IV)

G. RGP (Group-V)

H. RPTP (Group-VI)

Figure- 10.4. Radiological images of rats with treated, nontreated and disease model.

10.7.2.2. Bone weight, bone volume and bone density:

Table-10.7 and figure-10.6 summarize the effect of OVX and treatment of AGP, RGP, APTP and RPTP on bone weight, bone volume and bone density. From the results, it was found that the weight of bone in the OVX group (OG) was significantly ($p<0.05$) less than the normal group (NG), which might be due to demineralization or resorption of bone, which leads to bone loss. During treatment (treated groups G-I to III), the bones were mineralized and recovered with normal bone composition or the anti-resorptive activity of ATO, which stimulate the bone remodelling process as normal. The anti-osteoporotic activity of ATO inhibits osteoclastic activity by inhibiting osteoclast differentiation and osteoblast apoptosis and stimulates bone formation, leading to an increase in bone weight as well as bone mass density [52]. The bone weight was higher in rats treated with AGP (G-II) and APTP (G-III) as compared to ATO marketed formulation (G-I) due to the increased bioavailability of the drug, which results in increased anti-osteoporotic activity. The results indicated that the bone weight was decreased by ovariectomy surgery. After treatment with RSNa loaded formulations (G-IV to VI), a significant ($p<0.05$) increase in the weight of bone was observed due to the anti-osteoporotic activity of RSNa, which inhibits bone resorption and demineralization as well as stimulates the bone remodelling process as normal. The recovery of bone weight was higher in RGP (G-V) and RPTP (G-VI) as compared to RSNa marketed formulation (G-IV) due to an enhanced bioavailability of RSNa, which subsequently increased its anti-osteoporotic activity. The anti-osteoporotic activity of RSNa inhibits bone resorption by osteoclastic apoptosis and stimulates osteoblastic activity, which helps bone formation, leading to an increase in bone weight as well as bone mass density [53].

The bone volume of the femur in OG was significantly ($p<0.05$) higher as compared to NG. This conclusion is based on the gain in body weight of OG. As compared to OG, bone volume was decreased in the treated group with AMF (G-I), AGP (G-II) and APTP (G-III). In case of the RSNa treated group (G-IV to VI), there was no significant ($p>0.05$) difference observed. The bone volume of the femur decreased after treatment with RSNa formulations, i.e., RMF (G-IV), RGP (G-V), and RPTP (G-VI) as compared to the OG group.

With respect to bone weight and bone volume, the OG exhibited significantly (p<0.05) lower values for the bone density of femur than did the NG. This indicates that the bone mass density is decreased by ovariectomy. The results showed that bone density was significantly (p<0.05) increased after treatment of ATO loaded formulations. This was happened due to either stimulation of bone formation activity or anti-osteoporotic property of ATO [54]. The bone density of rats treated with AGP (G-II) and APTP (G-III) was higher as compared to the ATO marketed formulation (G-I). A significantly (p<0.05) increased in bone density was observed after treatment with RMF (G-IV), RGP (G-V), and RPTP (G-VI) due to the anti-osteoporotic or anti-resorptive properties of RSNa. The bone density of RGP (G-V) and RPTP (G-VI) was higher as compared to RMF (G-IV) due to enhanced bioavailability, which subsequently enhanced the anti-osteoporotic efficacy of RSNa.

On the basis of results, it was concluded that the ATO and RSNa loaded formulation i.e., AGP (G-II), RGP (G-V), APTP (G-III) and RPTP (G-VI) enhanced anti-osteoporotic activity as compared to ATO (G-I) and RSNa (G-IV) marketed formulation.

Table- 10.7. Analysis of bone weight, bone volume and bone density for bone samples

Groups	Drug treated group	Weight of bone (mg/mm)	Bone volume (mL)	Bone density (gm/mL)
NG	-	25.51 ± 2.22	0.68 ± 0.07	1.46 ± 0.17
OG	-	17.21 ± 1.50	0.79 ± 0.04	00.93 ± 0.03
G-I	AMF	18.94 ± 1.52*	0.72 ± 0.07*	1.04 ± 0.17*
G-II	AGP	22.30 ± 2.07*	0.74 ± 0.03*	1.29 ± 0.08*
G-III	APTP	21.00 ± 2.21*	0.71 ± 0.09*	1.11 ± 0.32*
G-IV	RMF	20.21 ± 1.69*	0.71 ± 0.06*	1.17 ± 0.26*
G-V	RGP	23.22 ± 2.51*	0.72 ± 0.02*	1.37 ± 0.17*
G-VI	RPTP	21.79 ± 0.64*	0.71 ± 0.05*	1.19 ± 0.22*

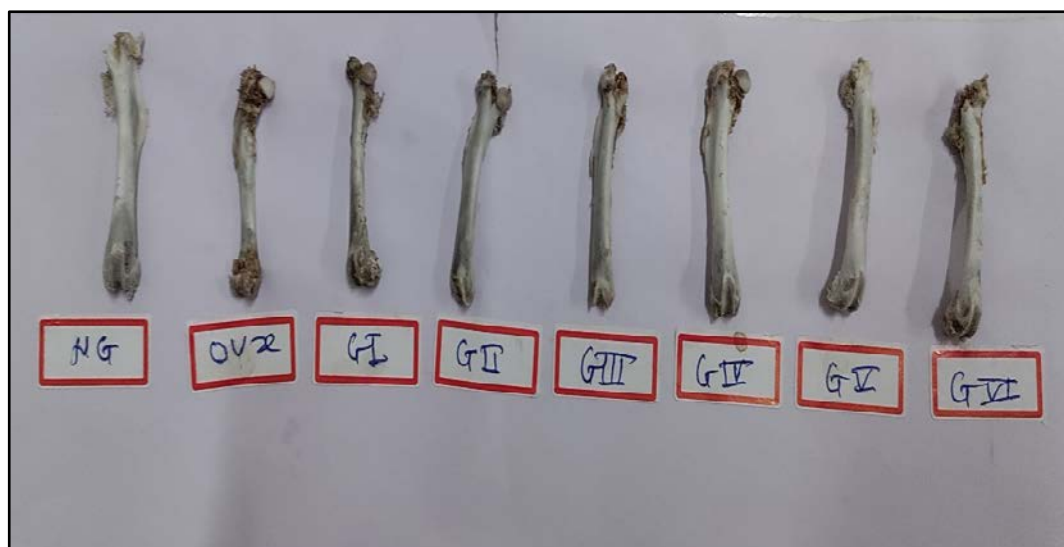* p < 0.05 as compared to OG.   (n=3, ± S.D.)

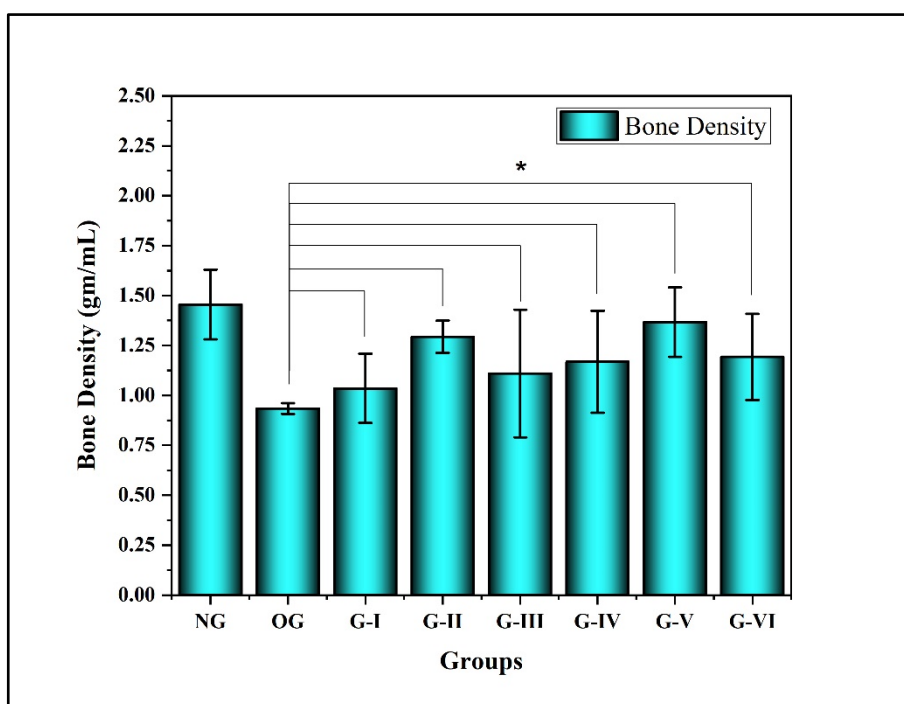Figure- 10.5. Bone samples isolated for analysis

*(p < 0.05)

Figure- 10.6. Change in bone density after treatment

10.7.2.3. Biochemical assay:

Table-10.8 and figure-10.7 represents serum level of calcium (a) and inorganic phosphorous (b) in NG, OG and after treatment (G-I to VI). Calcium and inorganic phosphate are considered bone mineral content markers. The results showed that the significant (p<0.05) decreased in the calcium and inorganic phosphorous serum level after ovariectomy surgery as compared to NG. The optimal range for calcium

serum level is 8- 12 mg/dL and inorganic phosphorous is 3-7 mg/dL [55, 56]. Ovariectomy increases Calcium (Ca) and inorganic phosphorous (iP) excretion in the urine while decreasing Ca and iP levels in the serum. It is likely related to the influence of oestrogen on intestinal calcium absorption that there is an increase in Ca and iP excretion [57]. The decrease in oestrogen may be responsible for Ca and iP being poorly absorbed in the gut, leading to more Ca and iP being excreted in the urine and faeces. Serum calcium deficiency is related to impaired ovarian function in producing oestrogen. Oestrogen may influence bone remodelling either directly or indirectly. Oestrogens influence calcium bioavailability as well as other endocrine activities related to bone remodelling. It has been demonstrated that ovariectomized rats experience due to the oestrogen lack associated with menopause [58, 59]. These diseases influence calcium absorption in the intestine, which is controlled by CaSRs (calcium sensing receptors) in the parathyroid glands. Ovariectomy may also cause a decrease in the number of vitamin D receptors in the jejunum, resulting in lower vitamin D cell response signalling in the gut and a decrease in intestinal calcium absorption [59-61]. After treatment, the serum calcium and inorganic phosphorous level was significantly increased as compared to OG. In case of ATO and RSNa loaded formulation, The calcium level is highest because it potentially elevates bone matrix formation and reduces bone breakdown [42, 62]. RSNa and ATO slows bone loss and improves bone mass, which avoids chances of osteoporosis. It was found that RSNa and ATO increases calcium loss from the blood while both improving absorption and bone deposition. The calcium and inorganic phosphorous serum level was significantly more in AGP (G-II), APTP (G-III), RGP (G-V), and RPTP (G-VI) as compared to ATO (G-I) and RSNa (G-IV) marketed formulation due to increasing bioavailability of ATO and RSNa by AGP (G-II), APTP (G-III), RGP (G-V) and RPTP (G-VI) resulted in increase in anti-osteoporotic effect. Based on the results, it was concluded that the AGP (G-II), APTP (G-III), RGP (G-V), and RPTP (G-VI) are potential drug delivery systems for the treatment of osteoporosis.

Table- 10.8. Serum profile of calcium and inorganic phosphorous

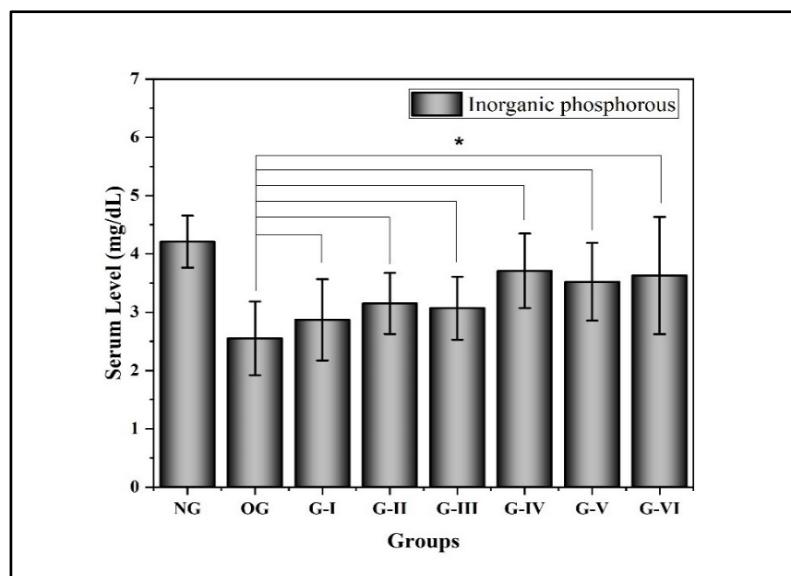| Groups	Drug treated group	Serum level (mg/dL)	
		Calcium	Inorganic phosphorous
NG	-	9.16 ± 1.02	4.21 ± 0.44
OG	-	5.38 ± 1.19	2.55 ± 0.63
G-I	AMF	6.63 ± 0.90*	2.87 ± 0.69*
G-II	AGP	8.37 ± 0.72*	3.07 ± 0.54*
G-III	APTP	8.06 ± 1.20*	3.52 ± 0.66*
G-IV	RMF	7.19 ± 1.06*	3.15 ± 0.52*
G-V	RGP	9.53 ± 1.03*	3.71 ± 0.64*
G-VI	RPTP	8.52 ± 1.22*	3.63 ± 1.00*

* $p < 0.05$ as compared to OG. (n=3, ± S.D.)
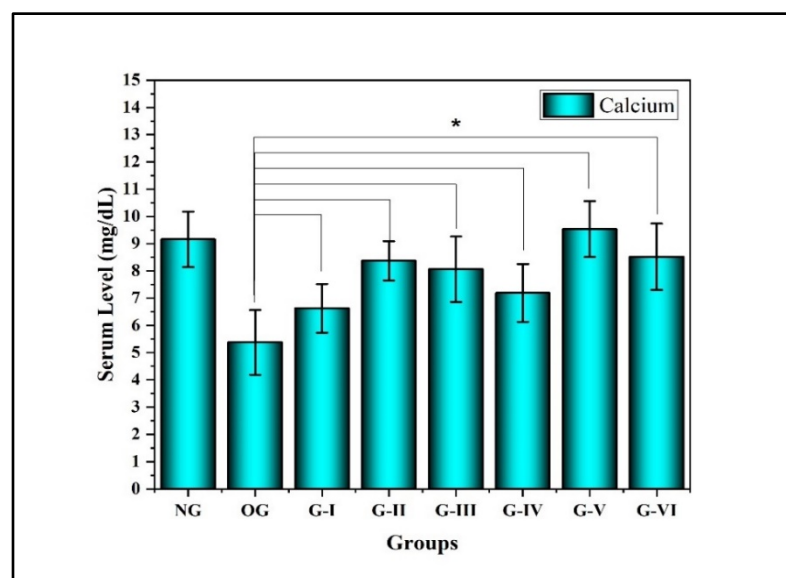
*($p < 0.05$)

(a)

*(p < 0.05)

(b)

Figure- 10.7. Serum calcium (a) and phosphate (b) level

10.7.2.4. Histopathology of bones:

The femur sections of rats were investigated for histological changes and shown in figure- 10.8 with different magnification 4X (a), 10X (b), 20X (c), 40X (d) and 60X (e). In the femur of normal group (figure- 10.8A), normal diaphysis microarchitecture with compact trabeculae was observed. Inner spongy bone showed a network of bony trabeculae separated by interconnected voids arranging bone marrow. It undergoes remodelling throughout life in response to mechanical loading, hormonal influences, and other factors. This remodelling process helps maintain bone strength and adapt to changing physiological demands. Sections of femur diaphysis showed an outer periosteum, the shell of cortical bone and endosteum, and bone marrow. The endosteum surface of the trabecular bone appeared smooth and lined with osteoprogenitor (*) cells and osteoblasts (OB). The cortical bone (#) is composed of a compact and dense bony structure with tightly packed layers of bone tissue called osteons or Haversian systems. Each osteon consists of mineralized extracellular matrix called lamellae. Within the lacunae of these lamellae, osteocytes, or bone cells, can be found. The bone trabeculae are composed of irregular bone lamellae and osteocytes inside the lacunae between the lamellar parts of the bone. The normal femur bone section

showed presence of a greater number of osteocytes which helps to balance bone remodelling process.

The femur of OVX group (figure- 10.8B) showed severe thinning of the trabecular, disappearance of growth plate and widening intertrabecular spaces due to loss of connectivity among the bone tissue. The femur displayed altered structural characteristics of trabecular bone (@), including abnormalities and erosion of the bone surface, deviating from its normal architecture. The broader spaces between the bone marrow ($) were observed, indicating widening of inter-bone marrow areas. The presence of osteoclasts was observed in the bone cavities (▲) and bone resorption (arrow ◣) was observed in the trabecular region. Osteoclasts were identified within the bone cavities, indicating their involvement in the process of bone resorption. The periosteum surface of cortical bone showed bone resorption. The OVX femur bone showed minimum osteocytes were presence which disbalanced the remodelling process.

After treatment of orally administered ATO (G-I) and RSNa (G-IV) (shown in figure- 10.8C and 10.8F, respectively), the section of femur showed slight reduction in erosion of bone surface and minimum bone cavitation was observed. A slight increase in the bone marrow in the treated groups was observed as compared to the OVX group. After the treatment of nanocarriers incorporated transdermal patch (G-II, G-III, G-V, and G-VI), significant increase in bone marrow was observed as compared to OVX group as well as G-I and G-IV (shown in figure-10.8D, 10.8E, 10.8G, and 10.8H). There was significant decrease in the erosion of bone surface and bone cavitation observed in the compact bone. In the femur of treated rats, the trabecular bone exhibited a normal architecture and density, indicating a healthy and intact structure. In the region of trabecular bone, only a few areas of bone resorption were observed, with most of the trabecular bone surrounded by regions of bone deposition. Distinct lines of bone deposition were prominently evident on the surface of the periosteum. The ruffled border, as well as the Harvesian system and bone matrix, showed a slight improvement, indicating constructive changes in the bone. The surfaces of both the periosteum and endosteum appeared smooth and were lined with osteoprogenitor cells, while only a few sites of erosion were observed. A significant degree of restoration was observed, characterized by the presence of a dense bone matrix and a thickened

ruffled border. After the treatment of developed formulation, significant recovery of osteocytes and osteoblast cells was observed, which retained the balance between bone formation and bone resorption.

On the basis of the results, it was concluded that the developed formulations more efficiently induced bone formation and reduced bone resorption, which helps in the treatment of osteoporosis.
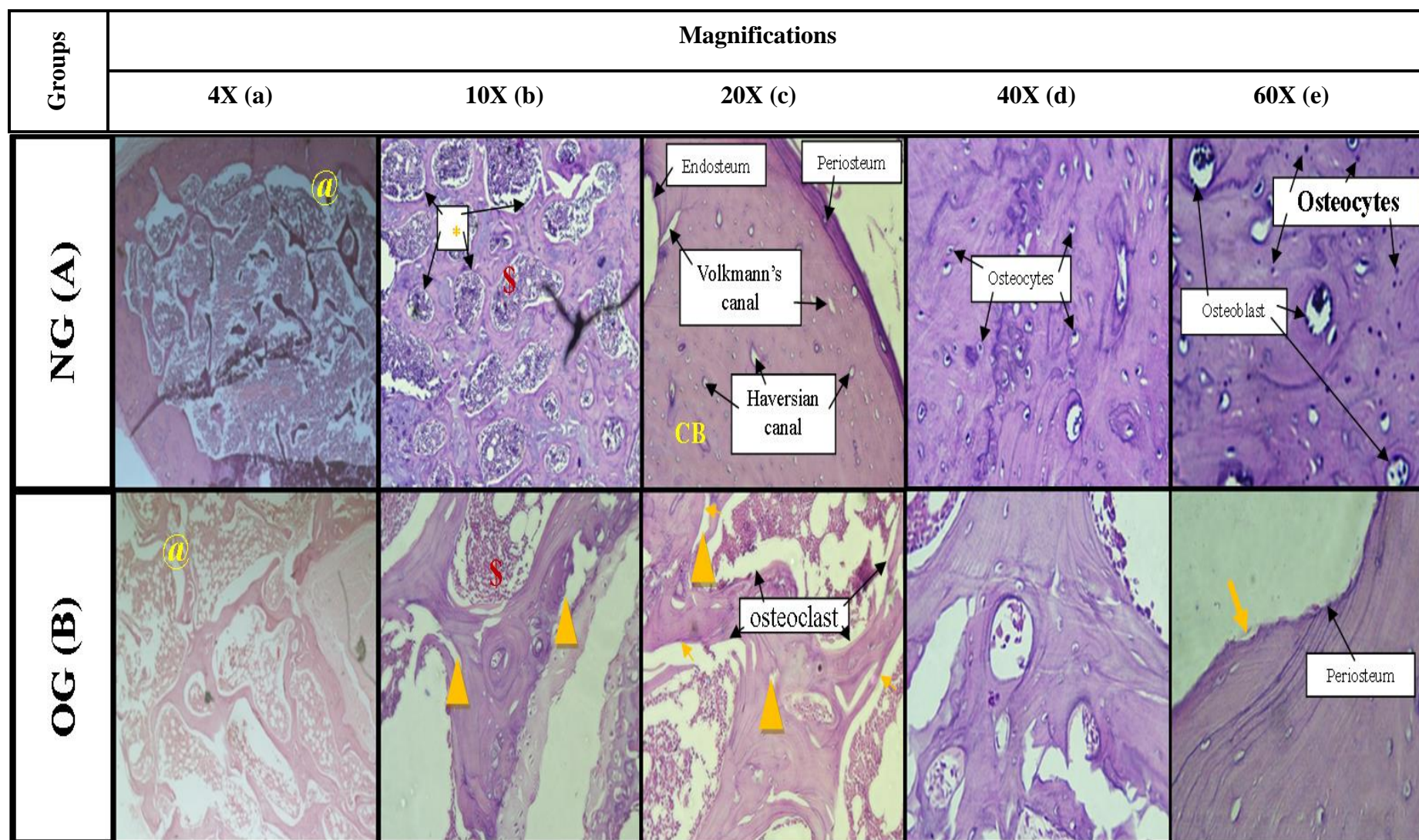
Groups	Magnifications				
	4X (a)	10X (b)	20X (c)	40X (d)	60X (e)
NG (A)					
OG (B)					

Figure- 10.8.1. Histopathological photomicrograph of femur bone samples from the normal group and the OVX group

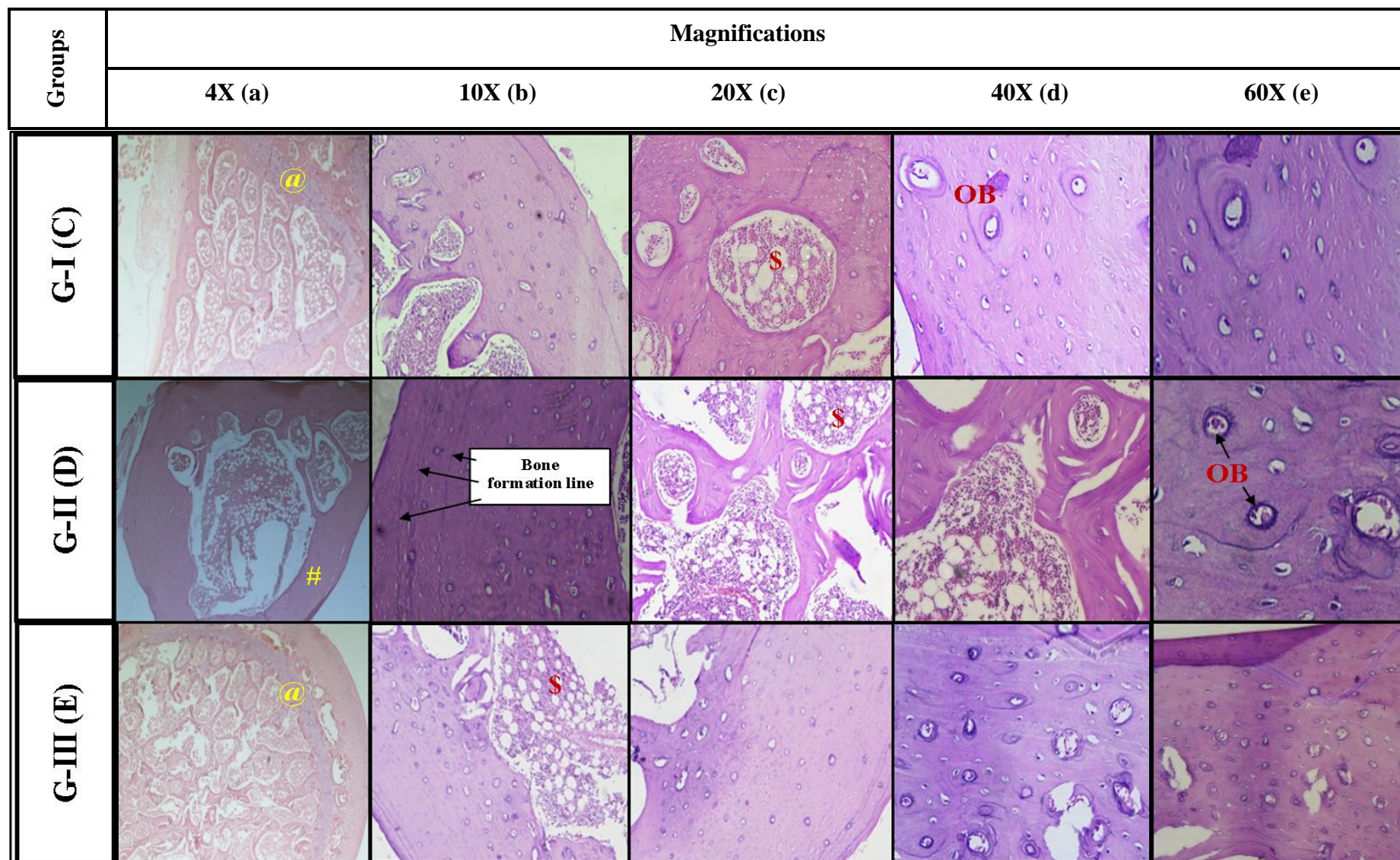| Groups	Magnifications				
	4X (a)	10X (b)	20X (c)	40X (d)	60X (e)
G-I (C)	@		$	OB	
G-II (D)	#	Bone formation line	$		OB
G-III (E)	@	$			

Figure- 10.8.2. Histopathological photomicrograph of femur bone samples from the ATO loaded formulations treated group
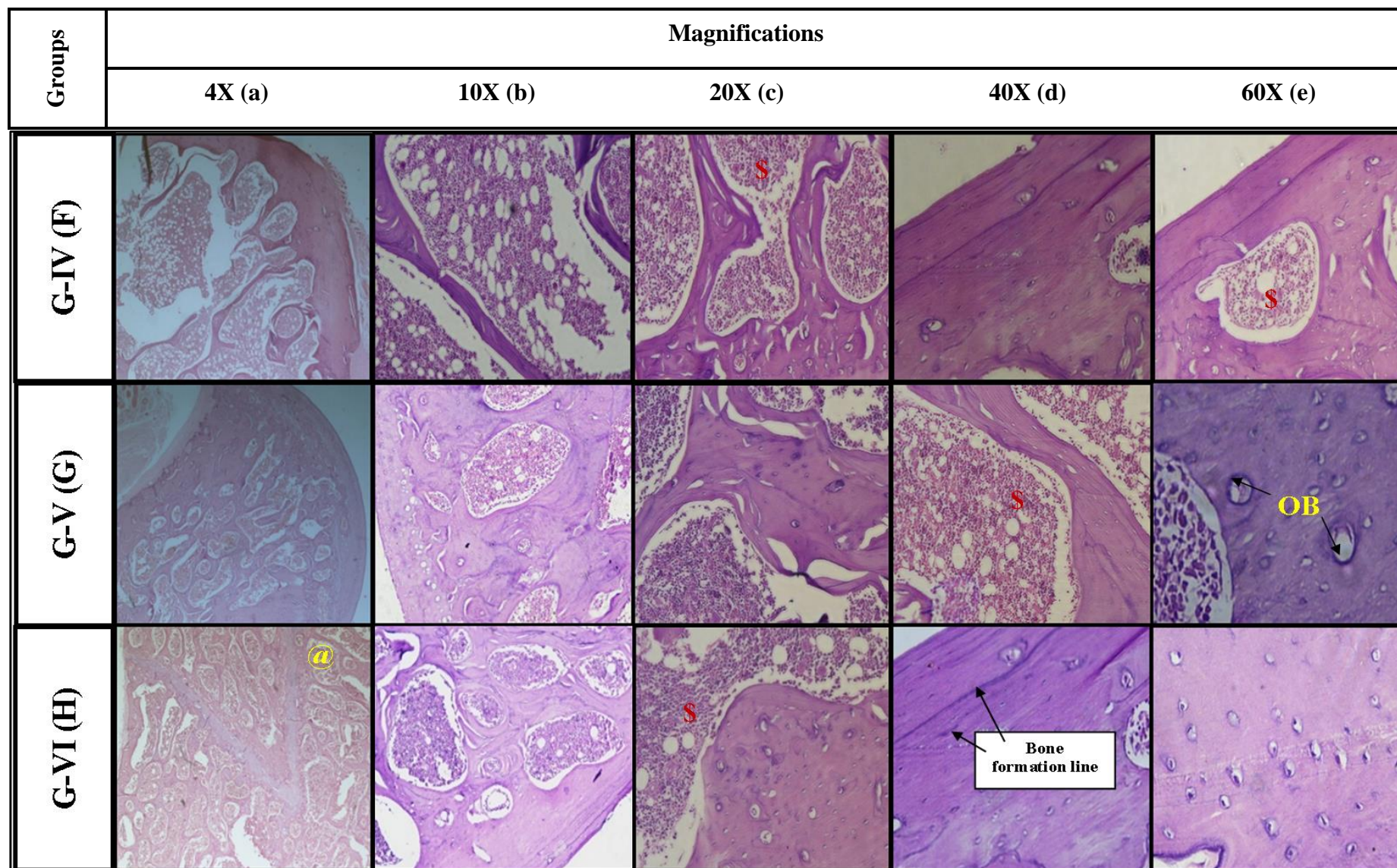
Figure- 10.8.3. Histopathological photomicrograph of femur bone samples from the RSNa loaded formulations treated group

Chapter 10 – In vivo studies

10.8. References:

1. Xie, Y., et al., *Atorvastatin-loaded micelles with bone-targeted ligand for the treatment of osteoporosis.* Drug Delivery, 2017. **24**(1): p. 1067-1076.

2. Kumar, N., et al., *Atorvastatin calcium loaded PCL nanoparticles: Development, optimization, in vitro and in vivo assessments.* RSC Advances, 2016. **6**(20): p. 16520-16532.

3. Ahmed, A.B., R. Konwar, and R.J.B.J.o.P.S. Sengupta, *Atorvastatin calcium loaded chitosan nanoparticles: in vitro evaluation and in vivo pharmacokinetic studies in rabbits.* Brazilian Journal of Pharmaceutical Sciences, 2015. **51**: p. 467-477.

4. AlKhani, M., A. Al-Laham, and M.A.J.I.J.P.S.R.R. Al-Mardini, *Simultaneous and precise HPLC method for quantification of atorvastatin in rat plasma and intestinal perfusion solution.* 2016. **38**(2): p. 70-4.

5. Jia, H.-J., W. Li, and K.J.A.c.a. Zhao, *Determination of risedronate in rat plasma samples by ion-pair high-performance liquid chromatography with UV detector.* Analytica Chimica Acta, 2006. **562**(2): p. 171-175.

6. Rawat, P., et al., *Three ply-walled microcapsules for enhanced pharmacokinetics of poorly absorbed risedronate sodium: novel stratagem toward osteoporosis.* Journal of Pharmaceutical Innovation, 2015. **10**: p. 130-139.

7. Jung, I.-W. and H.-K.J.I.J.o.N. Han, *Effective mucoadhesive liposomal delivery system for risedronate: Preparation and in vitro/in vivo characterization.* International Journal of Nanomedicine, 2014. **9**: p. 2299.

8. Rawat, P., et al., *Revisiting bone targeting potential of novel hydroxyapatite based surface modified PLGA nanoparticles of risedronate: pharmacokinetic and biochemical assessment.* International Journal of Pharmaceutics, 2016. **506**(1-2): p. 253-261.

9.   Suthar, N., J. Desai, and H.P.J.A.P. Thakkar, *Investigation on Potential of Chitosan Nanoparticles for Oral Bioavailability Enhancement of Risedronate Sodium.* AAPS PharmSciTech, 2021. **22**: p. 1-10.

10.   Lahoti, S.R.J.A.J.o.P., *Synergistic iontophoretic drug delivery of risedronate sodium in combination with electroporation and chemical penetration enhancer: Inâ€ vitro and inâ€ vivo evaluation.* Asian Journal of Pharmaceutics, 2015: p. 171-177.

11.   Li, S., et al., *Preparation, characterization, pharmacokinetics and tissue distribution of solid lipid nanoparticles loaded with tetrandrine.* AAPS PharmSciTech, 2011. **12**: p. 1011-1018.

12.   Kim, J.S., et al., *Enteric-coated tablet of risedronate sodium in combination with phytic acid, a natural chelating agent, for improved oral bioavailability.* Eur J Pharm Sci, 2016. **82**: p. 45-51.

13.   Turner, R.T., et al., *Animal models for osteoporosis.* 2001. **2**(1): p. 117.

14.   Jee, W. and W.J.J.M.N.I. Yao, *Overview: animal models of osteopenia and osteoporosis.* 2001. **1**(3): p. 193-207.

15.   Kusamori, K., et al., *Development of a novel transdermal patch of alendronate, a nitrogen-containing bisphosphonate, for the treatment of osteoporosis.* 2010. **25**(12): p. 2582-2591.

16.   El-Nabarawi, N., et al., *Atorvastatin, a double weapon in osteoporosis treatment: an experimental and clinical study.* 2017: p. 1383-1391.

17.   Turner, R.T., G.L. Evans, and G.K.J.E. Wakley, *Reduced chondroclast differentiation results in increased cancellous bone volume in estrogen-treated growing rats.* 1994. **134**(1): p. 461-466.

18.   Zhou, J., et al., *Effects of combined treatment with ibandronate and pulsed electromagnetic field on ovariectomy-induced osteoporosis in rats.* 2017. **38**(1): p. 31-40.

19. Sahana, H., et al., *Improvement in bone properties by using risedronate adsorbed hydroxyapatite novel nanoparticle based formulation in a rat model of osteoporosis.* 2013. **9**(2): p. 193-201.

20. Boyd, S.K., et al., *Monitoring individual morphological changes over time in ovariectomized rats by in vivo micro-computed tomography.* 2006. **39**(4): p. 854-862.

21. Abiramasundari, G., et al., *Ethnomedicine based evaluation of osteoprotective properties of Tinospora cordifolia on in vitro and in vivo model systems.* 2017. **87**: p. 342-354.

22. Yang, L., R.J.N.M.M. Zhang, and I.T.A.f.A.-A. Diseases, *Xiaoyun Li1†, Yan Cui2†, Qing Lin1, Panpan Wang3, 4, Rumeng Chen 1, Xiaofeng Zhu2, 3.* 2022.

23. Jacques, L.S., *Efeitos da suplementação de extratos de linhaça e/ou amoreira sobre o sistema ósseo de ratas ovariectomizadas.* 2022.

24. Cao, H., et al., *Effect of icariin on fracture healing in an ovariectomized rat model of osteoporosis.* 2017. **13**(5): p. 2399-2404.

25. Yousefzadeh, N., et al., *Ovariectomized rat model of osteoporosis: a practical guide.* 2020. **19**: p. 89.

26. Vhora, I., *Osteoporosis Treatment: A Genomic Approach.* 2016, Maharaja Sayajirao University of Baroda (India): India. p. 405.

27. Cho, C.-S., et al., *Anti-osteoporotic effects of mixed compositions of extracellular polymers isolated from Aureobasidium pullulans and Textoria morbifera in ovariectomized mice.* 2018. **18**: p. 1-15.

28. Kim, M.Y., et al., *Metabolic activities affect femur and lumbar vertebrae remodeling, and anti-resorptive risedronate disturbs femoral cortical bone remodeling.* 2021. **53**(1): p. 103-114.

29. Khajuria, D.K., R. Razdan, and D.R.J.J.o.O.S. Mahapatra, *Zoledronic acid in combination with alfacalcidol has additive effects on trabecular microarchitecture and mechanical properties in osteopenic ovariectomized rats.* 2014. **19**(4): p. 646-656.

30. Khajuria, D.K., et al., *Osteoprotective effect of propranolol in ovariectomized rats: a comparison with zoledronic acid and alfacalcidol.* 2013. **18**(5): p. 832-842.

31. Wu, C.-C., et al., *Calcium phosphate cement delivering zoledronate decreases bone turnover rate and restores bone architecture in ovariectomized rats.* 2012. **7**(3): p. 035009.

32. Stern, J. and W.J.C.C.A. Lewis, *The colorimetric estimation of calcium in serum with O-cresolphthalein complexone.* 1957. **2**(6): p. 576-580.

33. Deokar, S.A., et al., *Serum calcium and phosphorus levels: a marker of disease activity in senile cataract patients.* 2018.

34. Okon, A.U., et al., *Correlation of parasite density and biochemical parameters in children with malaria infection in Calabar, South-South Nigeria.* Egyptian Pediatric Association Gazette, 2022. **70**(1): p. 27.

35. Hokazono, E., et al., *Development of a new measurement method for serum calcium with chlorophosphonazo-III.* 2009. **46**(4): p. 296-301.

36. Gyanewali, S., et al., *Formulation development and in vitro–in vivo assessment of protransfersomal gel of anti-resorptive drug in osteoporosis treatment.* 2021. **608**: p. 121060.

37. Muñoz, M.A., M. Balón, and C.J.C.c. Fernandez, *Direct determination of inorganic phosphorus in serum with a single reagent.* 1983. **29**(2): p. 372-374.

38. Denney, J.W. and L.W. Denney, *Inorganic phosphate assay, and reagents therefor.* 1970, Google Patents.

39. Carvalho, L., T. De Koe, and P.J.R. Tavares, *An improved molybdenum blue method for simultaneous determination of inorganic phosphate and arsenate.* 1998. **1**(1).

40. Leyva, J.M., M.H. Artiga, and M.L.J.R.i.A.C. Chaves, *Determination of inorganic phosphate in urine samples: a review.* 1994. **13**(2): p. 99-126.

41. Nam, S.H., et al., *Topically administered Risedronate shows powerful anti-osteoporosis effect in ovariectomized mouse model.* 2012. **50**(1): p. 149-155.

42. Santhosh, S., et al., *Improved treatment efficacy of risedronate functionalized chitosan nanoparticles in osteoporosis: formulation development, in vivo, and molecular modelling studies.* 2019. **36**(4): p. 338-355.

43. Soliman, M.E., et al., *Star-shaped poly (oligoethylene glycol) copolymer-based gels: Thermo-responsive behaviour and bioapplicability for risedronate intranasal delivery.* 2018. **543**(1-2): p. 224-233.

44. Mukherjee, D., et al., *Improvement of bone microarchitecture in methylprednisolone induced rat model of osteoporosis by using thiolated chitosan-based risedronate mucoadhesive film.* 2018. **44**(11): p. 1845-1856.

45. Paliologo, T., et al., *Effects of swimming associated with risedronate in osteopenic bones: An experimental study with ovariectomized rats.* 2015. **78**: p. 40-44.

46. Hou, Y., et al., *Solid-in-oil nanodispersions as a novel delivery system to improve the oral bioavailability of bisphosphate, risedronate sodium.* European Journal of Pharmaceutical Sciences, 2020. **155**: p. 105521.

47. Bhattarai, N., et al., *PEG-grafted chitosan as an injectable thermosensitive hydrogel for sustained protein release.* 2005. **103**(3): p. 609-624.

48. Moolakkadath, T., et al., *Preparation and optimization of fisetin loaded glycerol based soft nanovesicles by Box-Behnken design.* 2020. **578**: p. 119125.

49. Boncheva, M., F. Damien, and V.J.B.e.B.A.-B. Normand, *Molecular organization of the lipid matrix in intact Stratum corneum using ATR-FTIR spectroscopy.* 2008. **1778**(5): p. 1344-1355.

50. Obata, Y., et al., *Infrared spectroscopic study of lipid interaction in stratum corneum treated with transdermal absorption enhancers.* 2010. **389**(1-2): p. 18-23.

51. Ogawa, K., et al., *Effects of combined elcatonin and alendronate treatment on the architecture and strength of bone in ovariectomized rats.* Journal of Bone and Mineral Metabolism, 2005. **23**(5): p. 351-358.

52. Ruan, F., Q. Zheng, and J.J.B.r. Wang, *Mechanisms of bone anabolism regulated by statins.* 2012. **32**(6): p. 511-519.

53. Ye, T., et al., *Protective effect of low-dose risedronate against osteocyte apoptosis and bone loss in ovariectomized rats.* 2017. **12**(10): p. e0186012.

54. Garrett, I.R. and G.R. Mundy, *The role of statins as potential targets for bone formation.* Arthritis Res, 2002. **4**(4): p. 237-40.

55. Moe, S.M., *Disorders involving calcium, phosphorus, and magnesium.* Prim Care, 2008. **35**(2): p. 215-37, v-vi.

56. Kim, G.-H., et al., *Serum calcium and phosphorus levels in patients undergoing maintenance hemodialysis: A multicentre study in Korea.* 2014. **33**(1): p. 52-57.

57. Walallawita, U.S., et al., *Potential role of lycopene in the prevention of postmenopausal bone loss: evidence from molecular to clinical studies.* 2020. **21**(19): p. 7119.

58. Abu-Taha, M., et al., *Menopause and ovariectomy cause a low grade of systemic inflammation that may be prevented by chronic treatment with low doses of estrogen or losartan.* 2009. **183**(2): p. 1393-1402.

59. Tsai, Y.-F., et al., *Long-Term Oral Toxicity and Anti-osteoporotic Effect of Sintered Dicalcium Pyrophosphate in Rat Model of Postmenopausal Osteoporosis.* Journal of Medical and Biological Engineering, 2017. **37**(2): p. 181-190.

60. Aminah, S., et al., *Consumption of elicited soybean sprout flour increases calcium level in serum of ovariectomized rats.* 2017. **36**(2): p. 94-101.

61. Poulsen, R.C. and M.C.J.N.R. Kruger, *Soy phytoestrogens: impact on postmenopausal bone loss and mechanisms of action.* 2008. **66**(7): p. 359-374.

62. Soliman, M.E., et al., *Star-shaped poly (oligoethylene glycol) copolymer-based gels: Thermo-responsive behaviour and bioapplicability for risedronate intranasal delivery.* International Journal of Pharmaceutics, 2018. **543**(1-2): p. 224-233.